LEGIBILITY NOTICE

A major purpose of the Technical Information Center is to provide the broadest dissemination possible of information contained in DOE's Research and Development Reports to business, industry, the academic community, and federal, state and local governments.

Although a small portion of this report is not reproducible, it is being made available to expedite the availability of information on the research discussed herein.

LA-UR

LA-UR--89-1592

DE89 012622

Received by

JUN 0 7 1989

Los Alamos National Laboratory is operated by the University of California for the United States Department of Energy under contract W-7405 ENG-36

TITLE Parallel Electric Fields in a Simulation of Magnetotail Reconnection and Plasmoid Evolution

AUTHOR(S) M. Hesse and J. Birn

SUBMITTED TO Proceedings of the Chapman Conference on the Physics of Magnetic Flux Ropes, Hamilton, Bermuda, 27-31 March 1989

DISCLAIMER

Los Alamos National Laboratory
Los Alamos, New Mexico 87545

Abstract We investigate properties of the electric field component parallel to the magnetic field ($E_\parallel$) in a three-dimensional MHD simulation of plasmoid formation and evolution in the magnetotail in the presence of a net dawn-dusk magnetic field component. We emphasize particularly the spatial localization of $E_\parallel$, the concept of a diffusion zone and the role of $E_\parallel$ in accelerating electrons. We find a localization of the region of enhanced $E_\parallel$ in all space directions with a strong concentration in the z direction. We identify this region as the diffusion zone, which plays a crucial role in reconnection theory through the local break-down of magnetic flux conservation. The presence of B_y implies a north-south asymmetry of the injection of accelerated particles into the near-earth region, if the net B_y field is strong enough to force particles to follow field lines through the diffusion region. We estimate that for a typical net B_y field this should affect the injection of electrons into the near-earth dawn region, so that precipitation into the northern (southern) hemisphere should dominate for duskward (dawnward) net B_y. In addition, we observe a spatial clottiness of the expected injection of adiabatic particles which could be related to the appearance of bright spots in auroras.

1. Introduction

A major characteristic of the magnetic reconnection process is the generation or existence of a localized region where the ideal MHD condition $\mathbf{E} + \mathbf{v} \times \mathbf{B} = 0$ breaks down, so that the global connection of plasma elements through magnetic field lines can change as these elements move through the system [*Axford*, 1984; *Schindler et al.*, 1988; *Hesse and Schindler*, 1988]. In idealized configurations, and in particular if symmetries are present, such a region, commonly called the "diffusion region", is associated with an X-type magnetic field topology [see, e.g., *Vasyliunas*, 1975] and with a magnetic null-line, or, more generally, a separator line defined by the intersection of separatrix surfaces between topologically distinct magnetic regions [e.g., *Sonnerup et al.*, 1984]. In the general three-dimensional case, however, the presence of magnetic nulls, neutral lines or separators is not necessary [*Schindler et al*, 1988]. The remaining characteristic of the diffusion region is therefore the electric field property, which requires in particular the localized presence of an electric field component parallel to the magnetic field for global changes of the magnetic connection [*Schindler et al.*, 1988; *Hesse and Schindler*, 1988]. In the idealized field geometries this parallel electric field in the diffusion region can be identified with an $E_{\parallel}$ along a separator or, if a magnetic neutral X-line exists, with an electric field along this X-line [*Sonnerup et al.*, 1984].

In this paper we will investigate the properties of the diffusion zone, and in particular its spatial extent and the consequences for adiabatic particle acceleration, on the basis of a three-dimensional MHD simulation of magnetic reconnection in a geomagnetic tail configuration without magnetic nulls. Details of the MHD simulation are described elsewhere

[*Birn and Hesse*, 1989a], an overview over the magnetic field evolution and the characteristic topology changes is given in this issue [*Birn and Hesse*, 1989b]. The evolution starts from a self-consistent tail equilibrium after *Birn* [1989], which includes a net dawn-dusk magnetic field component B_{yN}, that breaks the symmetry around the midnight meridian and the equatorial planes. Despite the strong influence of this field component on field line structures and topological connections, the evolution of the system remains similar to the symmetric case, showing plasmoid formation and ejection, starting at about 100 Alfvén times.

2. Enhancements of Parallel Electric Fields

Using a general concept of magnetic reconnection (general magnetic reconnection (GMR)), *Schindler et al.* [1988], and *Hesse and Schindler*, [1988] found that in systems without zeros of **B**, magnetic reconnection with global effects requires the presence of parallel electric fields in the diffusion zone with

$$\Phi = \int_{\text{fieldline}} E_{\parallel}\, ds \neq 0 \tag{1}$$

where the integration extends along a field line through the diffusion zone, and s is the arc length coordinate.

In view of this theory the question arises, whether the simulations of plasmoid evolution show the presence of a diffusion zone with this property. In the simulation, the resistivity η was chosen to be constant. This might suggest that a possible reconnection zone, defined by the spatial extent of $E_{\parallel}$ enhancements, were spread all over the simulation box rather that being localized. It is therefore of interest to investigate the spatial distribution of $E_{\parallel}$ during the simulation run.

We start our analysis with the investigation of the temporal variation of $E_{\parallel}$ during the simulation, looking first at the variation of $E_{\parallel}$ in the center of the plasma sheet, where the maximum $E_{\parallel}$ is found. Fig. 1 shows the variation of $E_{\parallel}$ along the x axis of the simulation box at different times. There is an obvious concentration of $E_{\parallel}$ with a peak at about $x = -10$, which starts immediately and saturates even before the plasmoid has started to form. Note that the maximum values attained by $E_{\parallel}$ do not vary much with time. This implies that some other, possibly geometric, effect must be responsible for generating

sufficiently high values of Φ for reconnection. We shall return to this problem in Section 3.

To demonstrate the further extent of the region of enhanced $E_{\|}$ Fig. 2 shows as an example the contour lines of $E_{\|}$ in the equatorial plane (a) and in the midnight-meridional plane (b) at $t = 165$ (time units normalized to typical Alfvén crossing times). The shaded area in Fig. 2a represents the region where $E_{\|}$ exceeds 50 % of its maximum value. The extent of this region in the y-coordinate direction is approximately given by $\Delta y \approx 10$, about half of the width of the simulation box. An estimate of the extent in the z-direction can be obtained from Fig. 3, which shows the variation of $E_{\|}$ and of the cross-tail current density j_y (in dimensionless units) with z at $t = 165$. The figure shows the concentration of j_y due to the compression of the plasma sheet in the reconnection region (Note that the z-coordinate is normalized by the initial scale of j_y.), and the even stronger concentration of $E_{\|}$ in the center of the current sheet. We estimate the width of the region where $E_{\|}$ exceeds about 50% of its maximum value to $\Delta z \approx 0.1$, so that the ratio of the volume of the enhanced $E_{\|}$ region to the entire volume is

$$\frac{\Delta x \Delta y \Delta z}{V} \approx 6 \times 10^{-4} \tag{2}$$

for this particular time.

The relative volumina of the enhancement region of $E_{\|}$ at times starting shortly before the plasmoid forms are plotted versus time in Fig. 4. Obviously, the relative size of the reconnection region (the region of enhanced $E_{\|}$) stays rather small at all times considered. Note that the limitation in the x- and y- direction and the strong concentration in z take place although the resistivity η is constant.

The fact that the volume of the diffusion zone is nonzero, implies that not a single field line but an entire rope of finite magnetic flux passes through it and exhibits enhanced $E_{\|}$ with possible consequences for acceleration of particles along these field lines.

3. Particle Acceleration

The quantity relevant for the acceleration along a field line is the integrated potential difference Φ, given by (1). Thus we extend our analysis to an integration of $E_{\parallel}$ along the field lines to find the distribution and the maximum values of Φ during the simulation run. As an example, Fig. 5a shows a typical spiralling field line. belonging to the plasmoid, at $t = 165$. Fig. 5b shows the variation of Φ along that specific field line. Note that there is a strong variation close to $s = 0$, i.e., close to the center of the field line, located on the x-axis at $x = -15$. The rather weak variation of Φ outside this central region is due to some field aligned currents at the plasma sheet boundary of the model, associated with parallel electric fields through the assumption of constant resistivity. The total voltage drop corresponds to about 14.4kV on this field line, using a lobe field strength of 40nT at the near-earth end, an initial plasma sheet scale size $L_z \approx 2R_E$ (half-thickness) and an Alfvén speed of 1000km/s.

The temporal variation of the maximum values of Φ during the simulation run is plotted in Fig. 6. It is obvious that the maximum values of Φ increase strongly during the plasmoid formation phase. At later times, while flux is still added to the plasmoid, the maximal Φ stays rather constant, around an average value of about 19kV. Note that the steep increase during the formation time occurs although the maximum of $E_{\parallel}$ does not vary much. This implies that the three-dimensional tearing mode changes the magnetic field geometry such that a set of field lines is picking up enough 'field aligned potential drop' to allow reconnection to proceed. This property can also be seen from the form of the field line in Fig. 5a. The part of that line of force closest to the x-axis almost lies in the

equatorial plane, due to the the fact that $\mathbf{B} \sim B_y \mathbf{e}_y$ there such that it picks up a rather high value of $\int E_{\parallel}\, ds$.

4. Electron Injection Patterns

Apart from the very late times, all plasmoid field lines in the present simulation connect with both ends to the boundary closest to Earth, as shown in the example of Fig. 5a. While it seems obvious that a concentration of $E_{\parallel}$ can act as a particle accelerator, up to energies of more than 10keV, it is not clear that particles can follow field lines after acceleration. Using the minimum magnetic field in the diffusion region of about 1nT, an electron energy of 15keV, and a plasmoid field line half length of $140R_E$ it is straightforward to estimate an electron Larmor radius to be less than $0.8R_E$, an $\mathbf{E} \times \mathbf{B}$ drift velocity to be at most of the order of 200km/s, and a typical travel time for an electron to the $x = 0$ plane of about 20s, which is much smaller than the evolution time of the system.

Therefore, a considerable part of the accelerated electrons can follow field lines to the end of the simulation box closest to the Earth. In order to investigate the distribution of these accelerated electrons at this boundary, we map the concentrations of field aligned voltage drops along the magnetic field to the $x = 0$ plane. Fig. 7 displays the contour lines resulting from this procedure for six different times of the simulation. The region of enhanced electron precipitation lies in the southern hemisphere for westward net B_y chosen in this simulation, and preferably on the dawn side (The regions bounded by the contour lines in the northern half-plane are no electron precipitation regions due to the direction of $E_{\parallel}$.).

At t=95 Alfvén times the distribution of enhanced Φ is still rather broad (panel (a)) with a maximum Φ of about 5kV. At later times (panels (b) -(f)), one can see an increasing concentration of the regions of field lines carrying higher potential drops, until, at times

greater than about 190 Alfvén times, only a very narrow clumpy region of the boundary plane is intersected by field lines with high potential drops. Assuming that these regions are actually regions of electron precipitation, we conclude that the temporal evolution of magnetotail reconnection may lead to an enhanced precipitation of energetic electrons in localized regions which decrease in spatial extent, resembling bright spot patterns as observed in the aurora.

Fig. 8 shows the footpoints of field lines that cross the x axis at the $x = 0$ plane. A comparison with Fig. 7 reveals that the folded structure of the foot points closely matches the main regions of enhanced precipitation patterns. The other regions are apparently made of footpoints of field lines of different types. As an example, Fig. 9 shows three different types of such field lines for $t = 212$. It shows that high values of Φ exist on some lobe-type magnetic field lines, and also on field lines that cross the equatorial plane just once near the "legs" of the plasmoid flux rope. High values of Φ on field lines of this kind can be interpreted as indications of magnetic reconnection on the flanks of the plasmoid.

The location of the precipitation region of adiabatic or nearly adiabatic particles relative to the equator depends on the sign of the net B_y (in the southern hemisphere for positive and in the northern for negative B_y). The electric field direction implies that the major part of the precipitation region of these electrons lies on the dawn side of the midnight meridional plane.

The ion behavior is impossible to predict without actually integrating particle orbits in the self-consistent fields. This is due to the fact that ions become nonadiabatic in the central plasma sheet region. Orbit calculations in ad-hoc field models [e.g., *Lyons and*

Spiser, 1982] indicate that such particles should become injected from the neutral sheet into both hemispheres with about equal probability, so that no north-south asymmetry is to be expected. The same result should hold for electrons if the net B_y is so small that they become non-adiabatic in the diffusion region, too.

While our present results suggest a north-south asymmetry of electron precipitation on the dawn side in connection with substorms, one must be aware that this property may be covered, or at least be superposed, by other influences on the electron precipitation pattern, such as electrostatic double layer structures [e.g., *Block*, 1984; *Reiff et al.*, 1988]. In this view, our results can be understood as providing indications of localized electron precipitation and pattern formation thereof to be caused by general magnetic reconnection in the tail leading to plasmoid formation and ejection.

Acknowledgments This work was supported by the U.S. Department of Energy through the Office of Basic Energy Sciences and by NASA. M. H. gratefully acknowledges support from the Los Alamos National Laboratory Director's postdoctoral program.

References

Axford, W.I., Magnetic Reconnection, in *Magnetic Reconnection in Space and Astrophysical Plasmas, Geophys. Monogr. Ser., vol. 30*, edited by E. W. Hones, Jr., p. 1, AGU, Washington D.C., 1984.

Birn, J., M. Hesse and K. Schindler, Filamentary structure of a three-dimensional plasmoid, *J. Geophys. Res., 94*, 241, 1989.

Birn, J., The distortion of the magnetotail equilibrium structure by a net cross-tail magnetic field, submitted to *J. Geophys. Res*, 1989.

Birn, J., and M. Hesse, MHD simulations of reconnection in a skewed three-dimensional tail configuration, submitted to *J. Geophys. Res.*, 1989a.

Birn, J., and M. Hesse, The magnetic topology of the plasmoid flux rope in a MHD simulation of magnetotail reconnection, this issue, 1989b.

Block, L., Three-dimensional potential structure associated with Birkeland currents, *Magnetospheric Currents, Geophys. Monogr. Ser., vol. 28*, edited by T. A. Potemra, p. 315, AGU, Washington D.C., 1984.

Hesse, M. and K. Schindler, A theoretical foundation of general magnetic reconnection, *J. Geophys. Res.*, *93*, 5559, 1988.

Lyons, L. R., and T. W. Spiser, Evidence for current sheet acceleration in the geomagnetic tail, *J. Geophys. Res.*, *88*, 2276, 1982.

Reiff, P. H., H. L. Collin, J. D. Craven, J. L. Burch, J. D. Winningham, E. G. Shelley, L. A. Frank, and M. A. Friedman, Determination of auroral electrostatic potentials using high- and low-altitude particle distributions, *J. Geophys. Res.*, *93*, 7441, 1988.

Schindler, K., M. Hesse and J. Birn, General magnetic reconnection, parallel electric fields and helicity, *J. Geophys. Res.*, *93*, 5547, 1988.

Sonnerup, B.U.Ö and 13 coauthors, in: Solar Terrestrial Physics: Present and Future, eds. D.M. Butler and K. Papadopoulos *NASA Ref. Publ. 1120, Washington, D.C.*, 1984, ch. 1

Vasyliunas, V.M., Theoretical Models of Magnetic Field Line Merging, 1, *Rev. Geophys. Space Phys.*, **13**, 303, 1975.

Michael Hesse and Joachim Birn, Los Alamos National Laboratory, Los Alamos, N.M. 87545

Fig. 1. Variation of the electric field component parallel to the magnetic field along the x-axis at different times. The times are normalized to typical Alfvén crossing times and the electric field unit is 0.2×10^{-3}V/m. The plots show a strong localization of $E_{\|}$ around $x = -10$.

Fig. 2. Contour lines of the parallel electric field in the equatorial plane (a) and the midnight meridional plane (b) at $t = 164.92$ Alfvén times. The enhanced contour line in the upper panel roughly indicates the line where $E_{\|}$ attains half the maximum value.

Fig. 3 Plot of the parallel electric field and the cross-tail current density versus z in the midnight meridian plane at x = -11.25 at t= 165. The axis labels give the units of $E_{\|}$, while dimensionless values of j_y are given by the absolute values of the axis labels.

Fig. 4. Plot of the relative volume of the diffusion region vs. time. Note that the relative volume of the region of enhanced $E_{\|}$ is very small during the entire simulation run, justifying the concept of a localized diffusion zone.

Fig. 5. (a) Typical spiralling plasmoid field line at time $t = 165$ Alfvén times. This field line was chosen to pass through the x-axis at $x = -15$. As it is typical for plasmoid field lines at this stage of the evolution, it connects to the boundary closest to Earth with both ends. (b) The lower panel shows the variation of Φ with arc length s along the field line in (a). The location of $s = 0$ corresponds to the x-axis at $x = -15$. Note that in the central region there is a steep increase in Φ due to the diffusion zone while the slow variation along the outer parts of the field line are due to some residual field aligned currents and the assumed constant resistivity.

Fig. 6. Temporal variation of the maximum values of $\Phi = \int E_{\parallel} ds$. At early times, the graph shows a steep increase in the maximum values, indicating that the three-dimensional tearing mode changes the geometry of the system in order to accommodate sufficiently high values of Φ for magnetic reconnection. After the formation of the plasmoid, the highest values of Φ stay around 19kV due to the fact that magnetic flux is continuously added to the plasmoid structure.

Fig. 7. Mapping of Φ to the end plane of the simulation box closest to Earth. The different panels show the contour lines gained by this procedure. The darker regions in the southern half in each panel indicate the region where field lines with higher values of Φ intersect this end plane, i.e., where the occurrence of accelerated electrons is most probable. Note that the plasmoid evolution causes a contraction of this region, from an initial rather broad diffuse pattern with rather low maximum values of Φ to a set of sharply bounded small regions with comparatively high maximum values of Φ.

Fig. 8 Footpoints at the $x = 0$ plane of field lines intersecting the x axis at varying values of x for six later times (solid lines) and for the initial equilibrium (dashed lines). Note that the footpoints of plasmoid field lines show a rather large separation in the y-direction. The folded structures of these footpoints coincide with the regions of high Φ in Fig. 7. The panels for the later times display an increased slope of the graph of the footpoints close to the center, corresponding to a dipolarization of the near Earth field.

Fig. 9 Typical field lines ending in the regions of high Φ at $t = 212$. The majority of field lines passing through the diffusion zone are spiralling plasmoid field lines, but high values of Φ can also be found on open lobe-like field lines and on the flanks of the plasmoid, on distorted field lines that topologically belong to the class of simple dipole field lines.

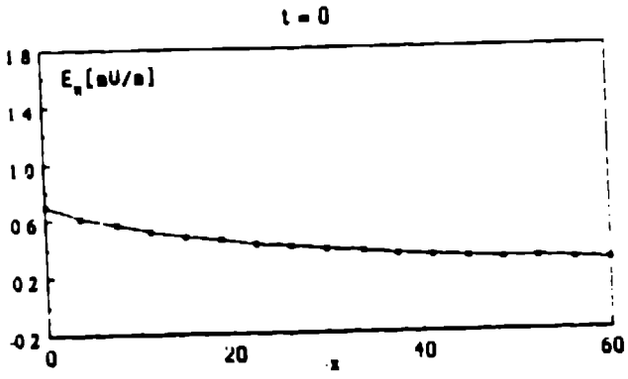
t = 0
E_z [mU/m]
1.8
1.4
1.0
0.6
0.2
-0.2
0
20
40
60
-x

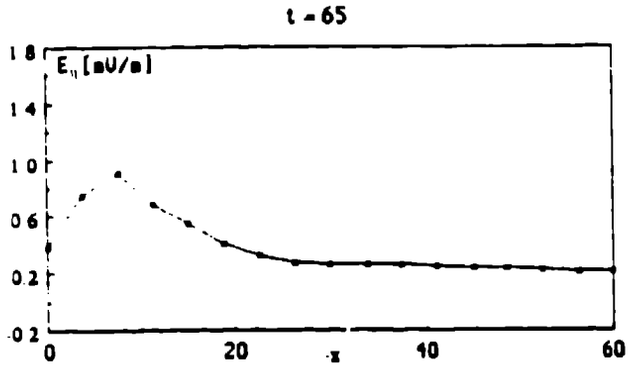
t = 65
E_z [mU/m]
1.8
1.4
1.0
0.6
0.2
-0.2
0
20
40
60
-x

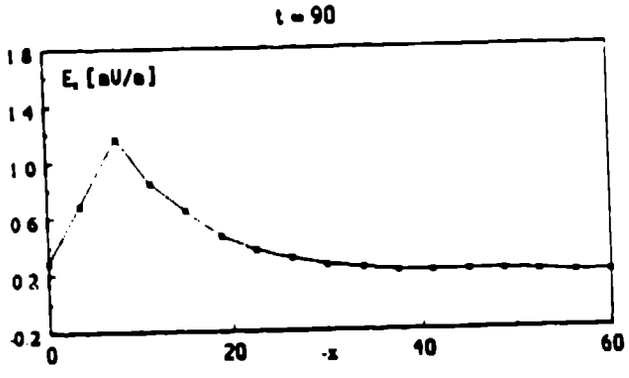
t = 90
E_z [mU/m]
1.8
1.4
1.0
0.6
0.2
-0.2
0
20
40
60
-x

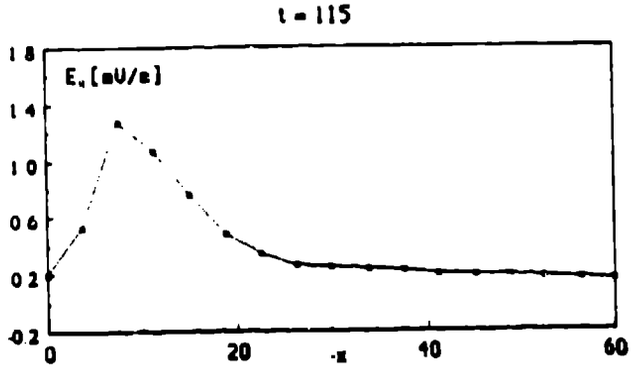
t = 115
E_z [mU/m]
1.8
1.4
1.0
0.6
0.2
-0.2
0
20
40
60
-x

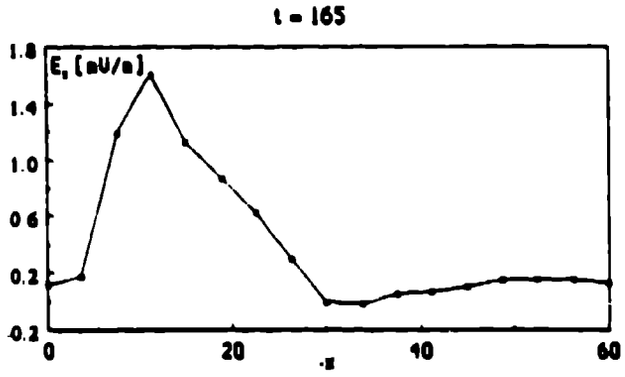
t = 165
E_z [mU/m]
1.8
1.4
1.0
0.6
0.2
-0.2
0
20
40
60
-x

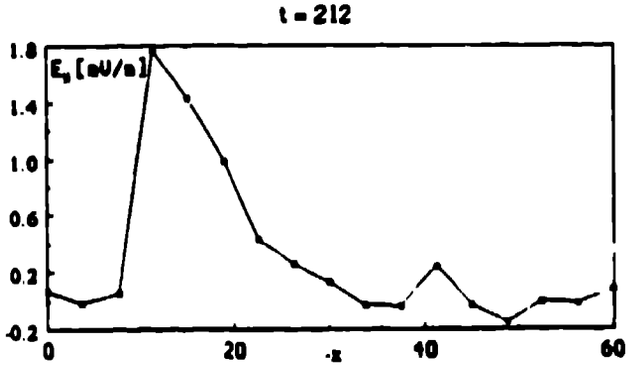
t = 212
E_z [mU/m]
1.8
1.4
1.0
0.6
0.2
-0.2
0
20
40
60
-x

Fig 1

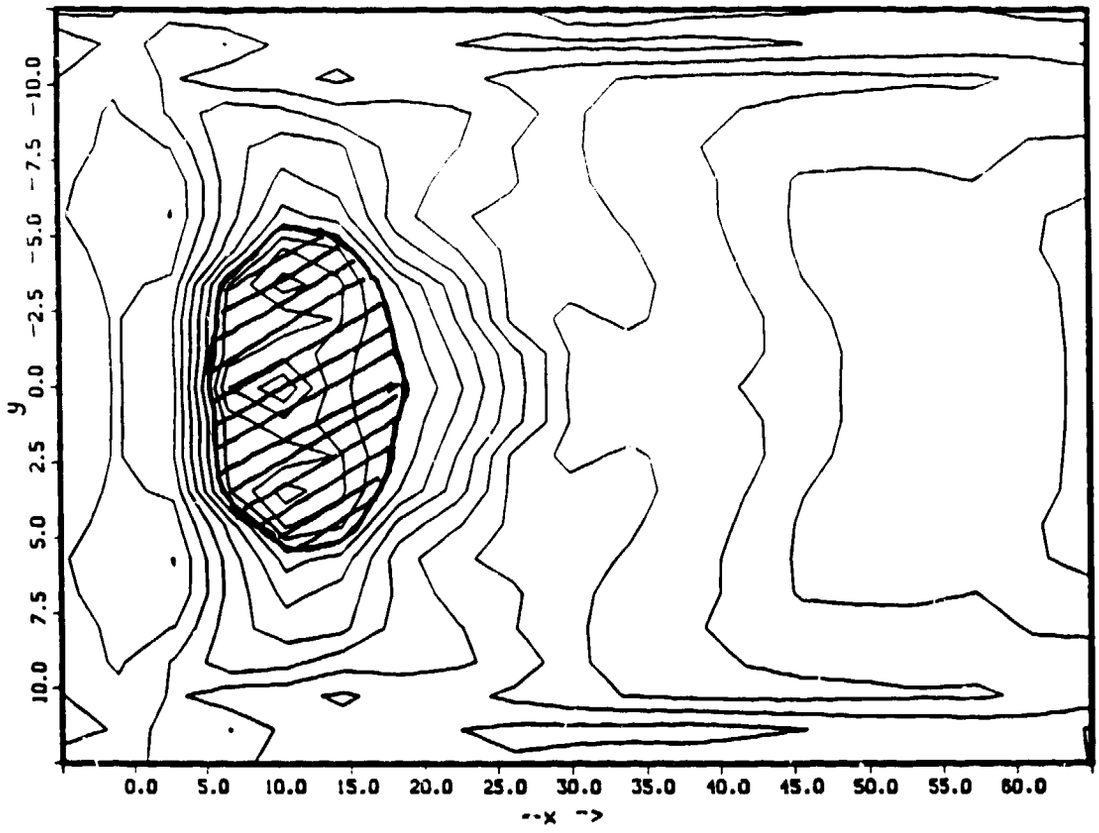
y
-10.0
-7.5
-5.0
-2.5
0.0
2.5
5.0
7.5
10.0
0.0
5.0
10.0
15.0
20.0
25.0
30.0
35.0
40.0
45.0
50.0
55.0
60.0
--x ->

a

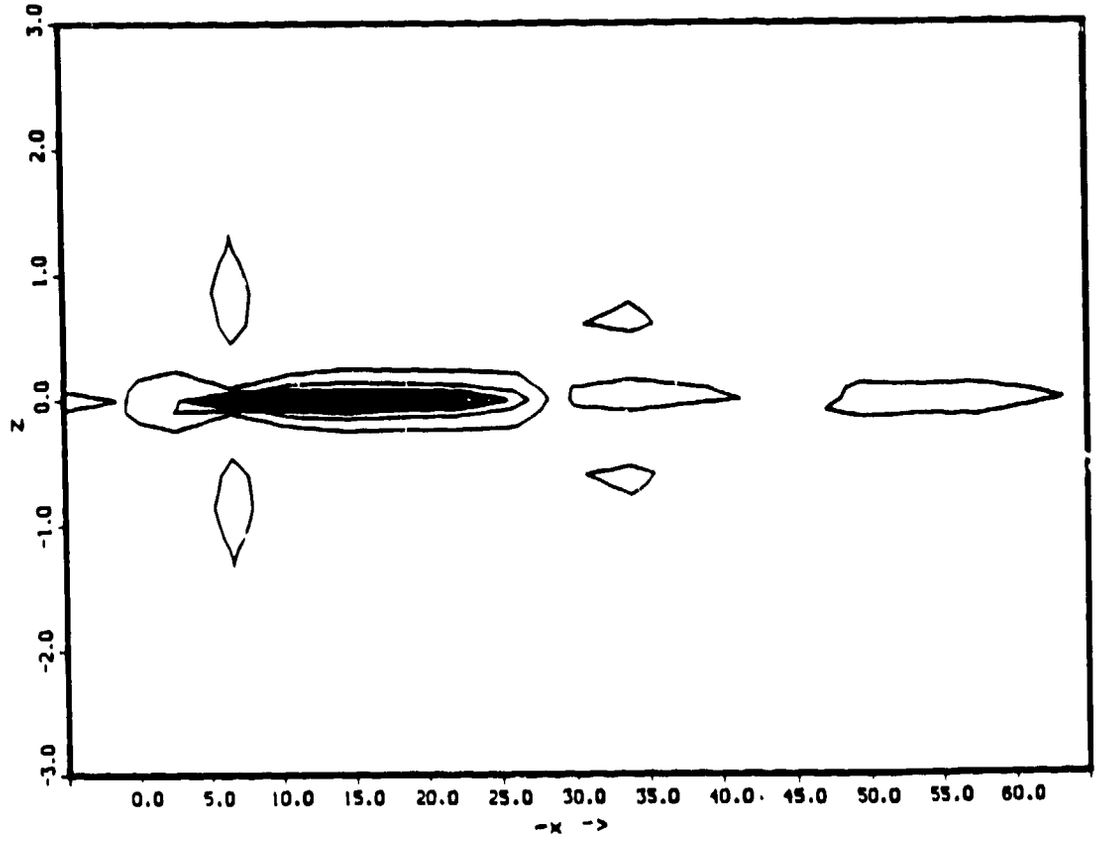
z
3.0
2.0
1.0
0.0
-1.0
-2.0
-3.0
0.0
5.0
10.0
15.0
20.0
25.0
30.0
35.0
40.0
45.0
50.0
55.0
60.0
-x ->

b

Fig. 2

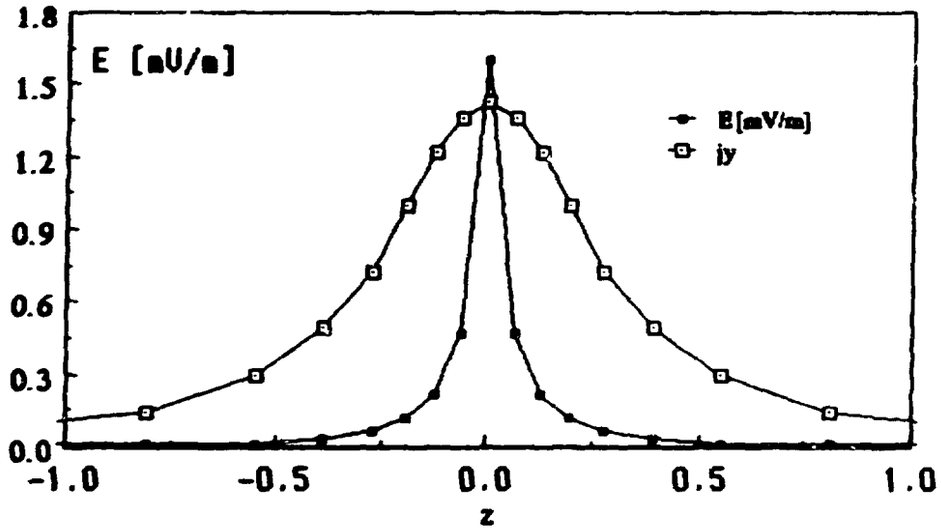

Fig 3

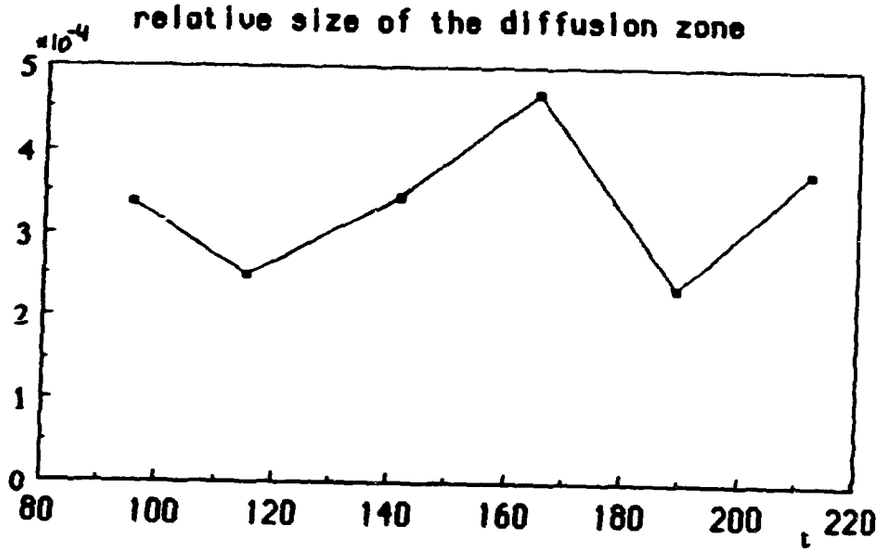
relative size of the diffusion zone
*10^-4
5
4
3
2
1
0
80
100
120
140
160
180
200
220
t

Fig 4

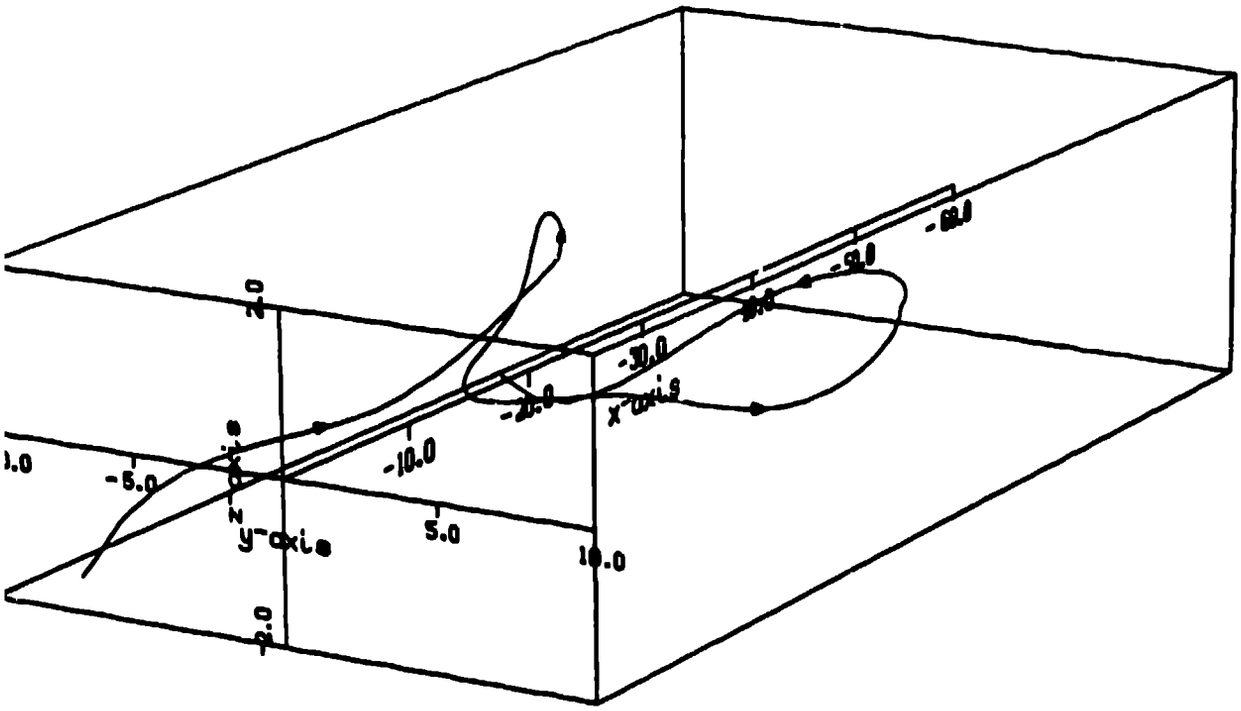
-10.0
-5.0
5.0
10.0
y-axis
x-axis

a

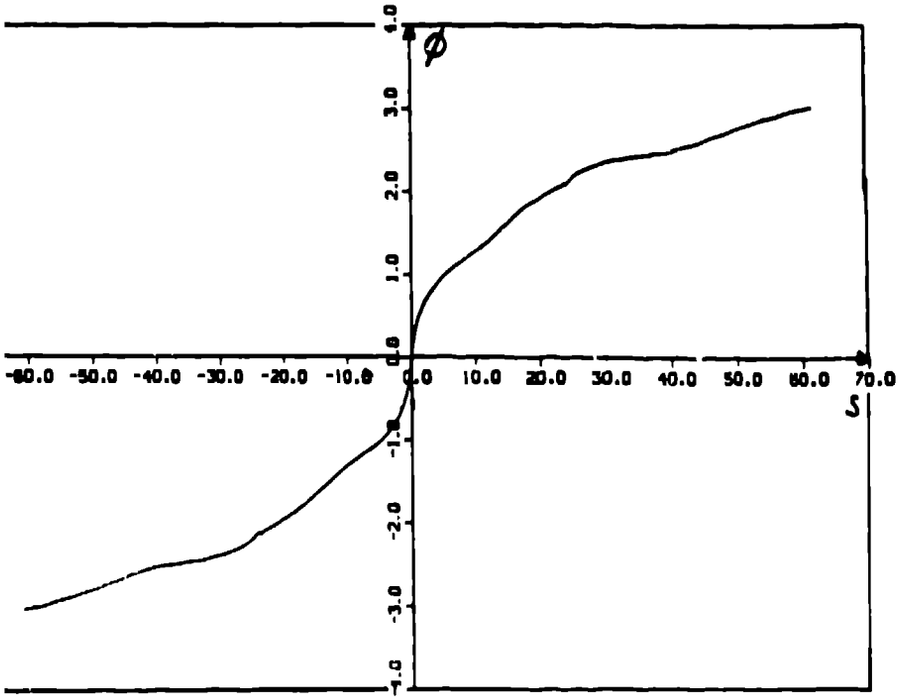
Φ
S
4.0
3.0
2.0
1.0
0.0
-2.0
-3.0
-4.0
-60.0 -50.0 -40.0 -30.0 -20.0 -10.0 0.0 10.0 20.0 30.0 40.0 50.0 60.0 70.0

b

Fig 5

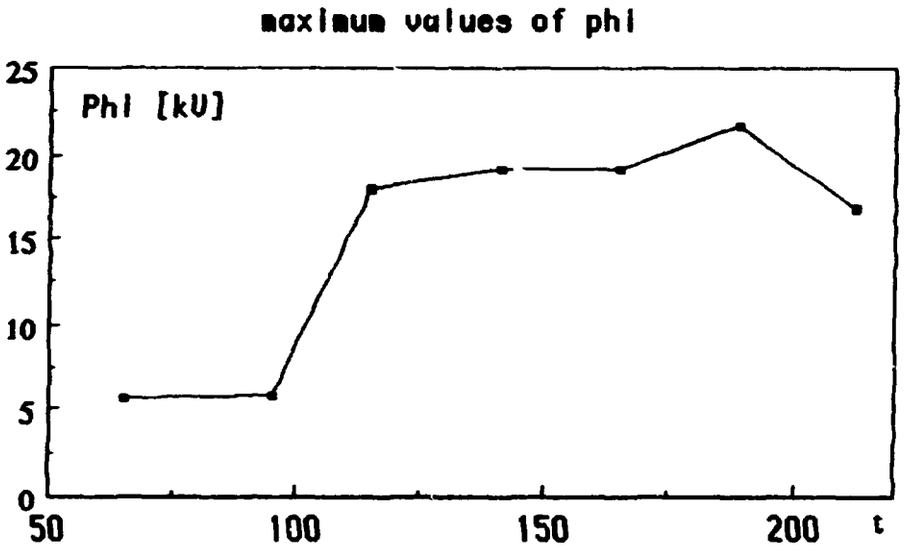

Fig 6

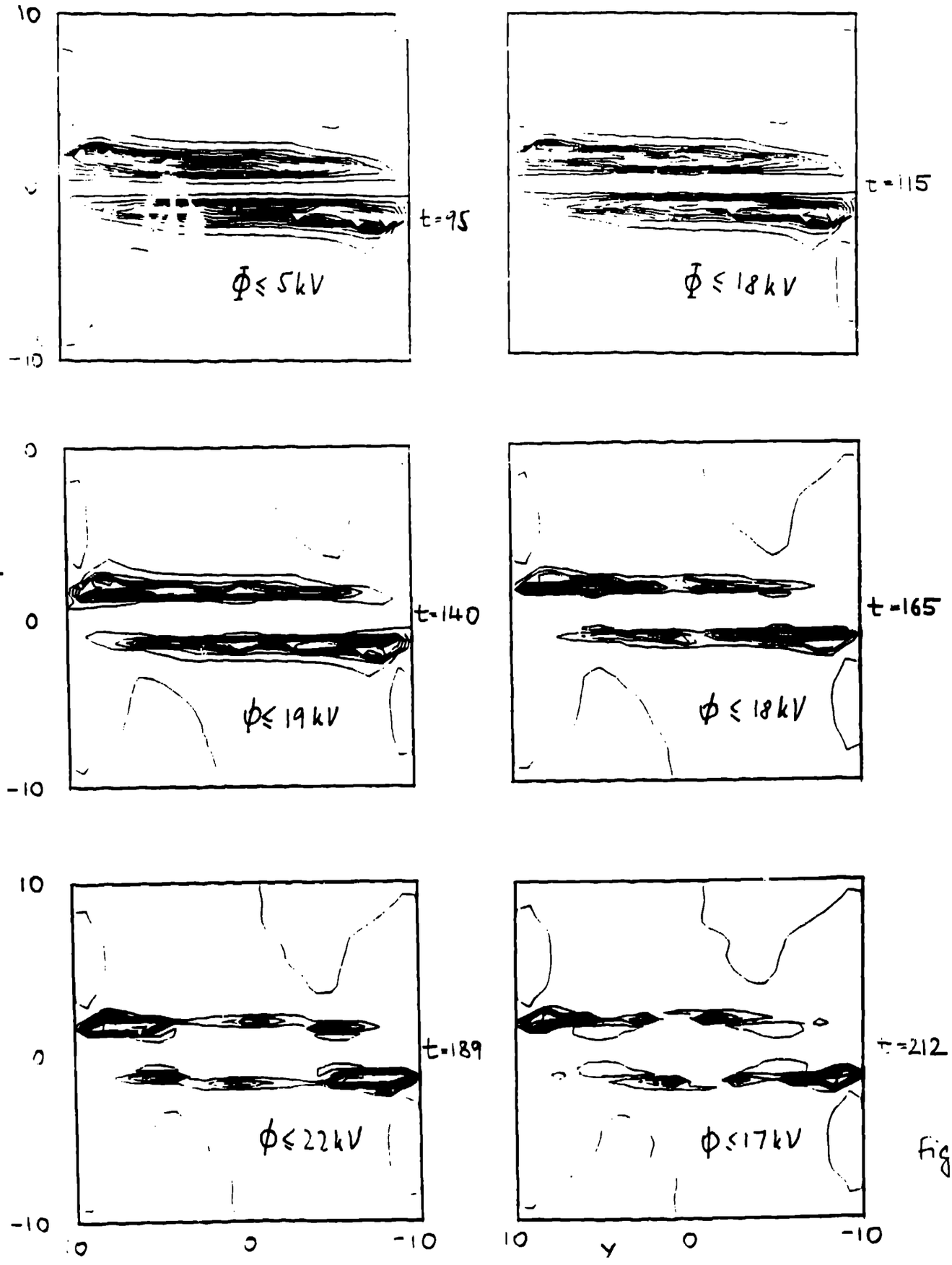
10
0
-10
t=95
Φ≤5kV
t=115
Φ≤18kV
z
t=140
Φ≤19kV
t=165
Φ≤18kV
t=189
Φ≤22kV
t=212
Φ≤17kV
10
0
-10
y

Fig 7

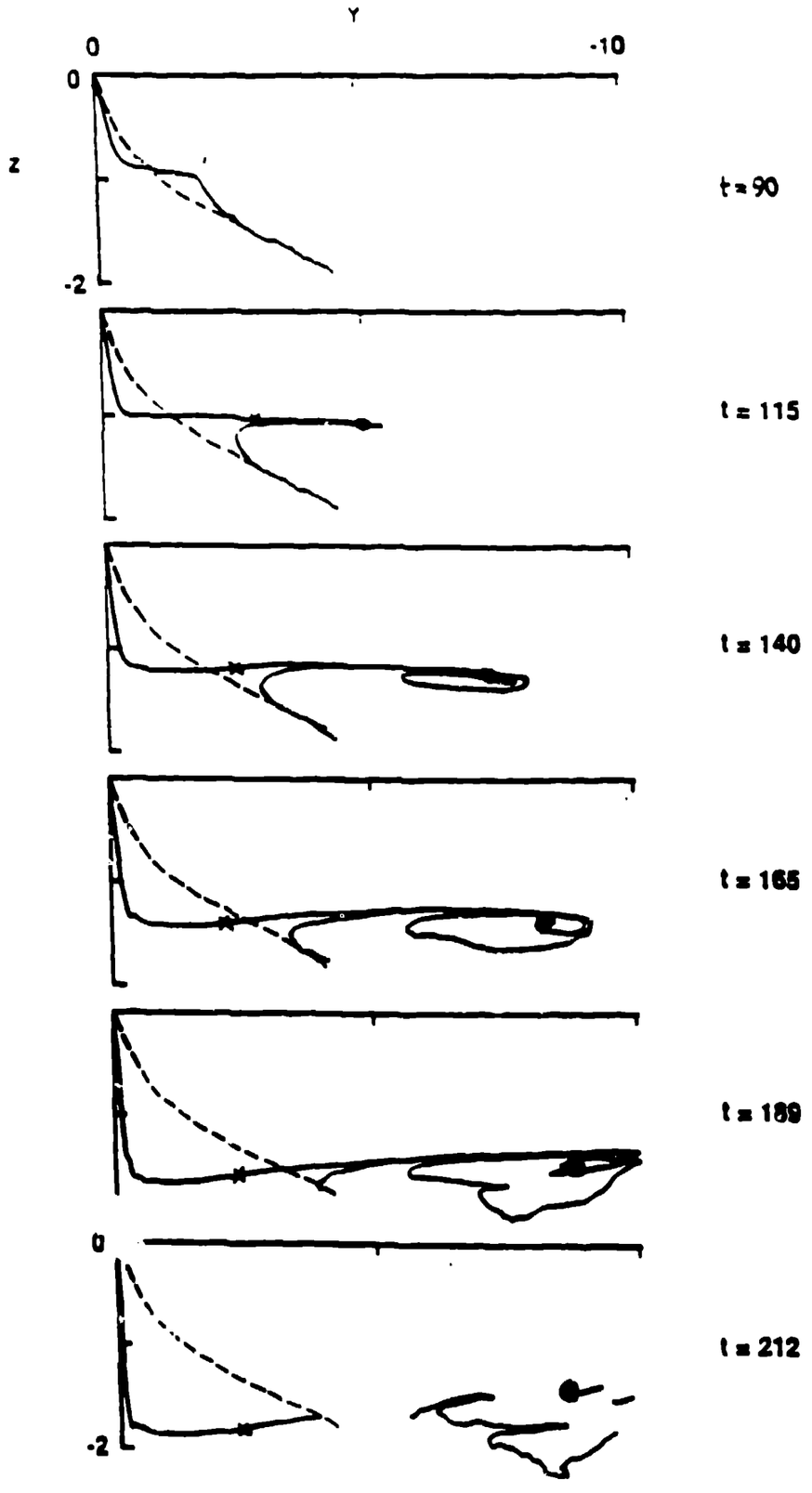

Fig. 8

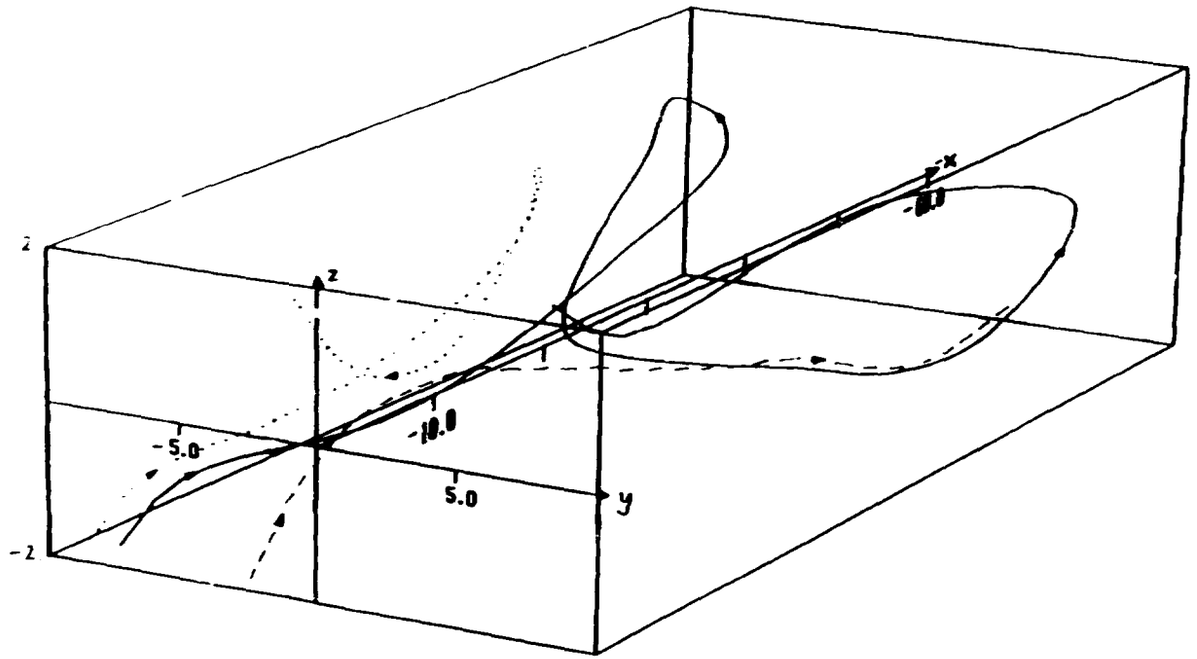

Fig 9